Toward a Physical Characterization of the Soviet/Russian Constellation of Molniya Satellites

Alberto Buzzoni[(1)], José Guichard[(2)], Giuseppe Altavilla[(3)], Alain Figer[(4)], Elisa Maria Alessi[(5)], Giacomo Tommei[(6)]

[(1)] INAF – OAS, Osservatorio di Astrofisica e Scienza dello Spazio, Via Gobetti 93/3, 40129 Bologna (Italy)
[(2)] INAOE, Instituto Nacional de Astrofísica, Óptica y Electrónica, L.E. Erro 1, Tonantzintla, Puebla, 72840 (México)
[(3)] INAF – OAR, Osservatorio Astronomico di Roma, Via Frascati 33, 00040 Monte Porzio Catone (RM) (Italy) & SSDC, Space Science Data Center, ASI Agenzia Spaziale Italiana, Via del Politecnico SNC, 00133, Roma (Italy)
[(4)] GEOS, Groupe Européen d'Observations Stellaires, 23 Parc de Levesville, 28399 Bailleau l'Evêque (France)
[(5)] CNR – IFAC, Istituto di Fisica Applicata "N. Carrara", Via Madonna del Piano 10, 50019 S.to Fiorentino (FI) (Italy)
[(6)] Università di Pisa, Dipartimento di Matematica, Largo B. Pontecorvo 5, 56127 Pisa (Italy)

ABSTRACT

We report on the extended 2014–17 observing campaign of the 43 surviving Soviet/Russian spacecraft Molniya, carried out at Mexican and Italian telescopes. Spectrophotometry and astrodynamical analysis have been carried out for all the dead payloads now in uncontrolled HEO orbit, in order to assess the possible differential age effect on the dynamical and reflectance properties of such a wide family of virtually identical orbiting objects, under the influence of Sun's radiation and gravitational and geomagnetic perturbation.

1 INTRODUCTION

The Molniya project (the name standing for the Russian "Lightning") inaugurated in the 60's the innovative concept of "satellite constellation" to deliver a communication service through the coordinated action of a set of satellites, not just relying on individual space relays. From a dynamical point of view, the adopted Molniya orbit (so christened after the name of the satellites) offered in fact a fully appealing alternative to the GEO option, the latter becoming practically ineffective for communication uses at latitudes $\gtrsim |70^o|$ (see, for instance, [1] for a comparative discussion). On the contrary a grid of HEO ($e \sim 0.7$) spacecraft enrouted along a much "closer"' ($a \sim 26500$ km or $P = 12$ hr) and inclined ($i \sim 63^o$) orbital path (see, e.g. [2]) was actually better suited to cover the wide-longitude and high-latitude extension of the Soviet Union (and present CSI republic), reaching up to latitude 83^o N with the Siberian military outposts.

Of course, a mandatory requirement for this orbital solution was to allow satellites to hover as long as possible the Soviet territory, a constrain achieved by a convenient choice of the argument of perigee (a value of $\omega \sim 270^o$ appeared to be a best option) such as to raise the satellite to nearly GEO altitude at its apogee over Russia. To safely maintain this configuration, however, the orbital plane has to be twisted such as to counteract the effect of J2 Earth gravitational dipole on ω and thus "freeze" the line of apsides. An inclination of the orbital plane about $i = \sin^{-1}(2/\sqrt{5}) \sim 63.4^o$ has proven to solve the problem (see, e.g. [3]), by vanishing the ω time derivative.

With these conditions, the resulting ground track of a nominal Molniya orbit looks like in Fig. 1. Note that a (draconic) period of $P = 12$ hr allows the satellite to reach its apogee in the northern hemisphere twice aday, and 180^o apart in longitude. In addition to the "Russian apogee"' (that allowed each Molniya satellite to be on-sight from the USSR for up to 10 hours), the supplementary North-American pass ensured, among others, a double visibility from the US and USSR and a stable link between Russia and Cuba, indeed a strategic advantage along the years of the Cold War. This special feature of the Molniya orbit was an argument in support of a space upgrade of the 1963 Moscow-Washington direct "hotline" [4] leading to set in place, in 1971, a safe satellite radio link by redundantly relying on four Soviet Molniyas 2 (then replaced with Molniyas 3 in 1996) and the US Intelsat 4F GEO network. After an experimental period, the satellite link became fully operational from 1978 until 2008. To this aim, from the US side, an earth-station was activated at Fort Detrick, MD, to track Molniya's transmissions, while the Intelsat relay was controlled from Etam, WV. On the USSR side, the Molniya/Intelsat link was controlled first from the city of Vladimir, close to Moscow, and then moved to Lviv (Leopolis) in Ucraina.

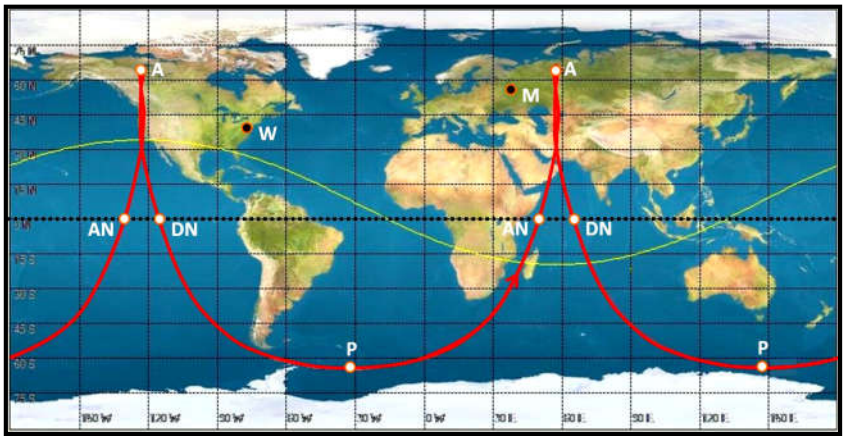

Fig. 1. An illustrative example of Molniya orbit ground track. Two 12-hr orbits are displayed to span a full day. The nominal orbital parameters are assumed, for illustrative scope, according to [2]. Note the extremely asymmetric location of the ascending (AN) and descending (DN) nodes, due to the high eccentricity of the orbit, and the perigee location (P), always placed in the Southern hemisphere. Along the two daily apogees (A), the satellite hovers first Russia and then Canada/US. The visibility horizon (i.e. the "foot print") attained from the "Russian apogee", is marked by the yellow line. Notice, in this example, that both Washington (W) and Moscow (M) are in sight from the spacecraft.

1.1 Launching timeline and spacecraft characteristics

Since the first launch of Molniya 1-01, on 1965 April 23 from Baikonur, a total of 164 spacecraft have been successfully delivered in HEO orbit with only one exception as for Molniya 1-S, placed in GEO orbit in 1974 [5]. The great majority of Molniya launches (some 136 out of 164) were carried out from the Russian Cosmodrome of Plesetsk (the remaining 28 missions being originated from Tyuratam/Baikonur). With its latitude of 63°N, Plesetsk was ideally located for Molniyas' enrouting in their inclined orbital plane at a fractional cost compared with similar payloads placed in equatorial GEO orbit [6].

Along the technical evolution of the Molniya program, three spacecraft series are recognized. Each series basically differs for the onboard technical equipment while only minor variations were introduced to the external bus. According to [7], the Molniya 1 series spanned the whole project lifetime, from 1965 to 2004, and included 94 successful missions. A total of 17 Molniya 2 missions were carried out between 1971-77, while 53 missions dealt with Molniya 3 spacecraft, between 1974 and 2003. In addition, 6 orbiting debris (all decayed) related to Molniya 1-05, 1-12, 1-17 and 3-23 main payloads have to be reported in the historic records [8]. The launch of Molniya 1-93, on 2004 February 18, led the program to its final completion.

As sketched in Fig. 2, a Molniya spacecraft consists of a Kaur-2 cylindrical bus coupled with a conical-shaped module hosting the Kdu-414 attitude thruster. The engine was fed by liquid propellant (Nitric Acid AK20F/UDMH) through a surrounding ring of small spherical pressure bottles. The thrust reached a specific impulse of 290 s [5]. As a fully distinctive feature, six solar pads stem from the satellite main body like petals, supplying the 1.3 kW onboard electrical power and giving the spacecraft its typical "daisy" shape. Two (redundant) high-gain parabolic (then conical) antennas were mounted on small steerable arms on opposite sides of the bus. The Kaur-2 bus was composed by a hermetically sealed, pressurized main section with 2.5 m^3 internal volume containing the equipment rack. Thermal control was assured by liquid gas cooling.

Satellite attitude was attained within a $\pm 10^o$ pointing accuracy [5] by means of a 3-axis gyroscopic stabilizers sensing the Sun direction and then acting on the thruster. This allowed the solar pads to continually face the Sun compensating for the ellipticity effects on the angular motion along the orbit (see [9] for a detailed analytical treatment of the problem). As the antennas had to be moved independently to dock and maintain the radio link with the ground station, Earth horizon was sensed by an on-board infrared detector [6]. The Molniyas sported a mass of 1500-1700 kg and a typical size of 1.6 m in diameter and 4.4 m in height, as far as only the satellite body (Kaur+Kdu modules) is considered. This figure raises however to 4.4x8.2x8.2 m with solar pads fully deployed. That is a reference size of 6.7 m, according to the geometrical mean of the three dimensions. The satellite active lifetime was entirely constrained by the frequency of attitude maneuvers, with the available propergol typically exhausted in 2 years, a limit that may have been extending up to 6 years in the most favorable cases [7].

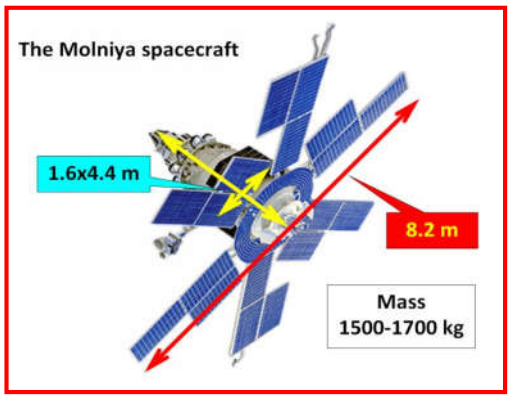

Fig. 2. A sketch of a Molniya spacecraft with its characteristic "daisy" look, as inspired by the six big solar panels. The spacecraft sports a size of 4.4x8.2x8.2 m, with a typical mass about 1500-1700 kg. Note that the two high-gain antennas, symmetrically placed at the two sides of the bus, are not displayed in this figure.

2 MOTIVATION OF THE STUDY & THE ITA-MEX OBSERVING CAMPAIGN

The study of the Molniya constellation offers in principle a unique opportunity to assess any differential ageing effect on the dynamical and reflectance properties of a wide family of virtually identical orbiting objects, under the effect of Sun's radiation and gravitational and geomagnetic perturbation. One has to consider, for instance, that the oldest surviving spacecraft, namely Molniya 2-09 and 2-10, were launched over four decades ago, in 1974, compared to the last spacecraft of the series, Molniya 1-93, launched in 2004 and already re-entered in 2016.

Late in 2014 we started our observing campaign aimed at characterizing from the photometric and spectroscopic point of view the entire constellation of the 43 Molniya satellites still surviving in orbit. Since the beginning of our project four satellites have decayed; for all of them however we still had a chance of collecting valuable data.

The "G.D. Cassini" 1.52 m telescope of INAF at the Loiano Observatory (Italy), was first allocated to the project, accompanied one year later, by the "G. Haro" 2.12 m telescope of the INAOE at the Cananea Observatory (Mexico). The longitude difference (about 120°) between the two observatories made both telescopes complementary to track the satellites along their double apogee location (either over Canada or Russia) under similar astronomical circumstances, with the targets always high at the NE-NW horizon in the sky. Along the full 2014-17 observing campaign, over 1/3 of the whole sample (16 objects) was actually tracked both from Mexico and Italy.

2.1 The Loiano dataset

The Cassini 1.52 m f/8 telescope was equipped with the on-board BFOSC camera which covered a field of view of 13.0x12.6 arcmin, imaged with a 1340x1300 back-illuminated EEV CCD with 15 μm pixel size. This led to a 0.58 arcsec/px plate scale across the field. Multicolor photometry was carried out in all the Johnson-Cousins BVR_cI_c bands. Along a total of 13 observing nights, between 2014 August 04 and 2017 May 29, imagery of a substantial fraction of the Molniya constellation (37 objects) was collected, that is about 3/4 of the whole sample, also adding unique or repeated low-res spectroscopy for 31 objects,.

Our strategy for imaging relied both on "trailing" and "on-target" observations. In the first case we let the target move across the CCD field during the exposure with the telescope in standard sideral tracking. This technique better reveals any quick luminosity change of the satellite and more easily allows one to assess possible periodicities in the tumbling properties of the body. On the other hand, "on-target" tracking greatly enhances the satellite detection as photon stacking leads to much higher S/N, even with shorter exposure time (see, e.g. [10] for a discussion).

In particular, the "on-target" tracking was obviously the mandatory requirement to carry out any spectroscopic observation of our fast-moving targets, crossing the sky at some 250-350 arcsec/min in excess to the sideral motion, even when caught close to the apogee. The spectroscopic data were especially collected along the 2016 observing runs. In its spectroscopic mode, the BFOSC camera was equipped either with grism GR4 or a nearly equivalent combination of the two grisms GR3+GR5, to sample in both cases the full wavelength interval λ 4000-9000 Å with a 4.0 Å/px dispersion, through a 5 arcsec-wide slit. As the slit width exceeded in any case the optical seeing figure,

the resolving power of our data was in fact constrained by the atmospheric seeing (typically about 1.5-2 arcsec FWHM). This led to an effective spectral resolution of 15 Å FWHM for our spectra, or an implied resolving power $R = \lambda/\Delta\lambda \sim 400$.

2.2 The Cananea dataset

Observations from Mexico started with the session of 2015 November 24, to which four other followed until 2016 March 10, for a total of 5 nights allotted to the project. The Haro 2.12 m f/12 telescope was equipped with the on-board LFOSC camera, providing a field of view of 10.0x6.0 arcmin, imaged with a 578x385 front-illuminated EEV P8603 CCD with 22 μm pixel size. This led to a 0.98 arcsec/px plate scale across the field. Johnson-Cousins BVR_cI_c multicolor photometry was carried out for a total of 20 objects of the Molniya population, providing for most of them a complementary photometry to Loiano observations, including 4 satellites not observed from Italy. The observing strategy forcedly relied on "trailing" imagery of the targets somewhat eased by the bigger collecting area of the telescope, compared to Loiano.

3 OBSERVING STRATEGY AND RESULTS

Basically three main fields of investigation were addressed with our observations. According to the expected lifetime of orbiting Molniyas, we are actually dealing with a population of demised non-cooperant spacecraft, tumbling in a fully uncontrolled way under the influence of gravitational and geo-magnetic perturbations. In this context, the "trailing" imagery allowed us to better constrain the tumbling properties of each object, while multicolor observations and spectroscopy provided important clues on the reflectance properties and "photometric signature" of the satellites. In addition, we took advantage of the exhaustive two-line elements (TLE) database available from NORAD [11] to assess the dynamical history of each spacecraft and carry out a detailed *ex-post* analysis of the combined role of atmospheric drag and lunisolar perturbations along the satellite's life until (in some cases) its final re-entry.

3.1 Tumbling properties

Telescope imagery in "trailing" mode is the ultimate tool to detect with exquisite detail Molniyas' spinning properties. In case of passive (non-cooperant) objects, one has to expect the body to eventually move in a so-called "flat-spinning" regime, by tumbling with a prevailing component around the major axis of Euler's inertial ellipsoid [12]. For the Molniya spacecraft, this rotation is about a normal direction to the spacecraft symmetry axis (see Fig. 2). Under Earth's gravity gradient, and other effects, the spin axis will slightly precess with time and the spin period has to slow down as long as the spacecraft interacts with Earth's magnetosphere by eddy-current dissipation [13]. This is especially the case for Molniyas, given their HEO orbit, that leads spacecraft to cross the Van Allen radiation belts at least four times aday. Repeated assessment of the spinning period over the years would therefore provide important clues on this perturbing effect.

An example of trailing observations of Molniya 1-63, from a 2016 observing session in Loiano, is shown in the left panel of Fig. 3. Over the 30 sec exposure time it is well evident a periodic change in satellite's luminosity, roughly on a 4-sec timescale. This trend can also be recognized in supplementary 2016 I-band observations of the same target, taken at Cananea, as shown in the right panel of the same figure.

A more thorough assessment of spacecraft's spin period(s) can be attempted, for instance, with the method of the phase-dispersion-measure (PDM) score [14], where for each period guess to fold data a merit parameter (aka nominally a "signal-to-noise ratio", S/N) is computed as a ratio between coherent and random magnitude change of the phased lightcurve. In particular, a direct estimate for the random variance of (phase-sorted) magnitude measurements (m_i) could be computed as $\sigma^2 = \Sigma(m_i - m_{i-1})^2/n$. At the same time, the total amplitude (A) of the (smoothed) lightcurve can simply derive from the plot, as a measure of the coherent trend of light variation. A fiducial S/N confidence level can eventually be attached to each lightcurve as $S/N = A/\sigma$. The result of our exercise for the full set of Cananea I-band frames of Molniya 1-63 is shown in Fig. 4, here below.

Just a glance to the plot emphasizes at least two important features. First, an outstanding peak can be recognized about $P \sim 4$ sec, with multiple alias values around 1/2x (namely ~2 sec) and 2x (i.e. ~8 sec), the latter actually with a similar statistical strength. Second, a set of viable periods tends to "cluster" around the P = 2, 4, 8 sec main pivots. This cluster structure directly derives from a subtle inherent bias dealing with the trailing observations. Again, a closer look to the right panel of Fig. 3 may help figuring out the effect.

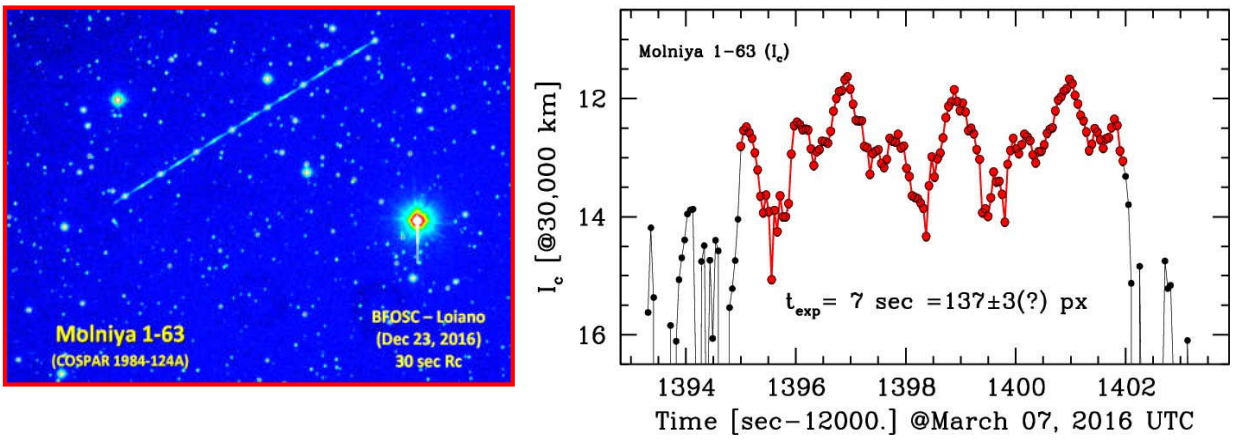

Fig. 3. (Left panel): a 30-sec R-band frame tracking Molniya 1-63 across the sky of Loiano, during a 2016 observing session. Note the repeated dot-dashed pattern along the satellite trace. (Right panel): the extracted track of Molniya 1-63 from an I-band LFOSC frame taken in Cananea, on 2016 March 7. The 7-sec exposure clearly shows a repeating pattern over timescales about 4 seconds. The very short (but finite) time for the CCD shutter to start/stop the exposure makes the exact "cut" of the track (both in pixel/time and magnitude) somewhat uncertain, as discussed in the text. The adopted satellite track, taking a total of 137 *bona fide* "switched-on" pixels, is marked in red for this example.

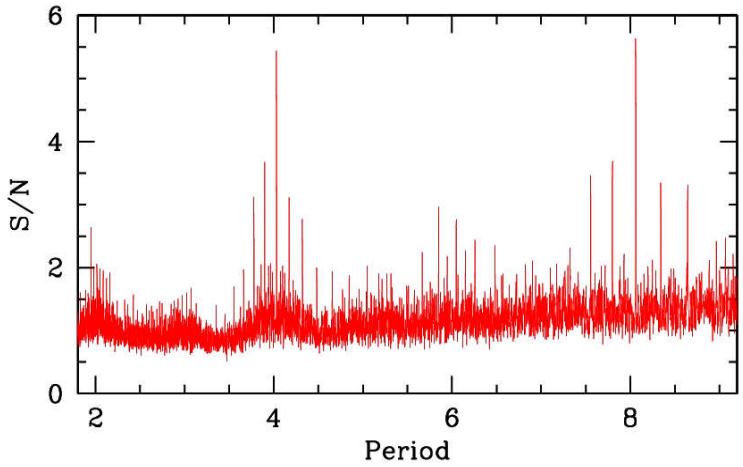

Fig. 4. A PDM score plot for a set of I-band frames of Molniya 1-63 (one of which is shown in the right panel of Fig. 3), in search for the likely periodicity values. Note the period clustering around the value of P~4 sec and its corresponding 1/2x and 2x "aliases" around P~2 and 8 sec, respectively, as discussed in the text. According to our analysis, the spacecraft appears eventually to spin with a period P = 4.031 sec.

In fact, while our shot was nominally a "sharp" 7.0 sec exposure, the short (but finite) time of shutter opening, combined with the underlying variation of the target luminosity, makes it difficult any exact "cut" of the genuine satellite track over the background. For the data in the figure one sees that a ±3 pixel uncertainty might still be an acceptable guess in locating the exposure start/end points along the total of 137 *bona fide* "switched-on" pixels (marked in red in the figure). Correspondingly, this reflects in a timeline uncertainty, that propagates to any inferred periodicity, so that dP/P ~ 3/137 ~ 2%. With these figures, even by combining several frames to increase the time baseline and refine the period, one has to carefully consider that any information on the "right" period definitely tends to "blur" within a lapse of 137/3 ~ 45 period cycles. For our example on Molniya 1-63, this is a time span of roughly 3 minutes. As a consequence, some ambiguity on the exact value of P cannot definitely be ruled out when observing the same target at a cadence of a few minutes, still retaining a cluster of "ancillary" periods surrounding the nominal solution in the periodogram.

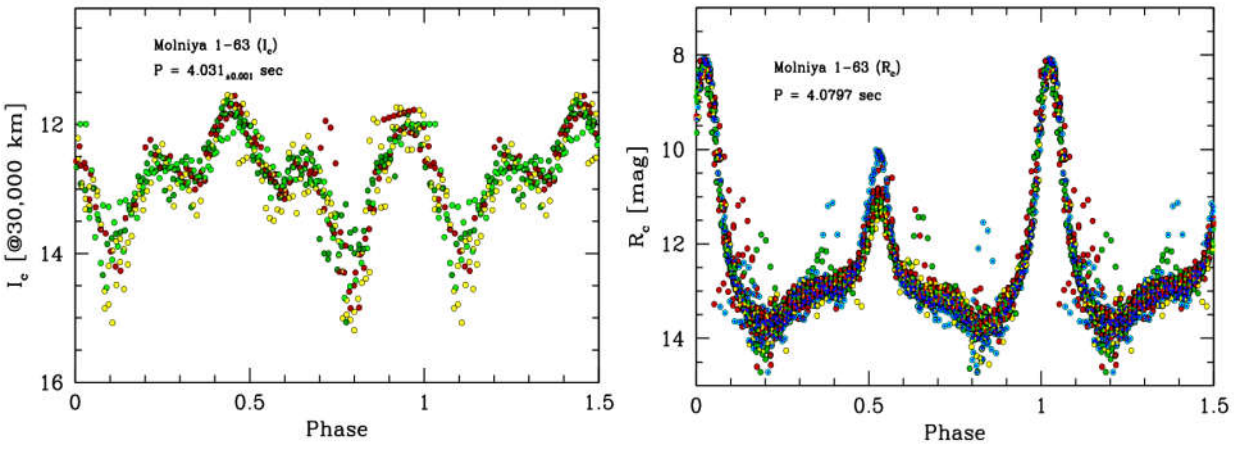

Fig. 5. The folded I- and R-band lightcurve of Molniya 1-63, as seen from Cananea (left panel) and Loiano (right panel), along two 2016 observing runs. In both cases (and throughout in this paper) apparent magnitudes are scaled to a fixed reference distance of 30,000 km. Note the quite different pattern, with the flashing behavior of the Loiano observations, as discussed in the text.

3.2 Lightcurves

According to Fig. 4, the Cananea I-band data of Molniya 1-63 could be folded with P=4.031 sec to obtain the lightcurve in the left panel of Fig. 5. To a closer analysis, the magnitude pattern seems a quite distinctive feature for the entire Molniya constellation, as evident for instance also in Fig. 6 for the supplementary cases of Molniya 2-09 and 3-42. Two prevailing peaks of luminosity can always be recognized in these lightcurves, exactly half a period apart, to be attributed to the solar pads assembly onboard the spacecraft. A more composite pattern is always evident, however, around one of the two main peaks (most likely that from the "rear" face of the solar pads), displaying much broader wings, as produced by the satellite bus, likely seen "in front" and under illumination. In addition, a couple of smaller "bumps", symmetrical to the main maximum, may be attributed to the two high-gain (often parabolic) steerable antennas onboard. Half a period later, the six "petals" of the solar pads are now "in front", and they may likely be shadowing the bus (and partly the antennas) thus leaving a sharper single peak, as displayed in the plots.

To some extent, the Fig. 6 lightcurve pattern may therefore be regarded as a genuine "photometric signature" of Molniya satellites, although a fully different behavior may set on under special illumination circumstances. An outstanding case, in this regard, is displayed in the right panel of Fig. 5, again for Molniya 1-63. In the latter case, the satellite appears dramatically brighter, reaching magnitude $R_c \sim 8$ at the primary maximum (around phase $\varphi \sim 1$ in the plot). In addition, the secondary peak (around $\varphi \sim 0.5$) now surmounts by far the bus broader bump with only a hint of the antennas signature. Clearly, the abrupt increase of spacecraft luminosity comes from the solar pad mirroring "something bright". A FWHM value about $\Delta\varphi \sim 0.6$ for the two main peaks in the lightcurve points to a quite broad illumination source, angularly extending some 20 deg across, as seen from the spacecraft. Our conclusion is therefore that Molniya 1-63 was in fact mirroring not the Sun but Earth (and most probably the Arctic Ocean) in daylight.

3.3 Colors and reflectance properties

In addition to spacecraft lightcurve and spinning properties, Molniya imagery taken through different photometric filters provides us with an important piece of information about the way the satellite's components reflect/scatter incoming light. On the same line, even long-slit reflectance spectroscopy provides a similar information but at more refined "panchromatic" detail. For their complexity, however, the latter are much more demanding observations as "on-target" telescope tracking is required to maintain the satellite steady inside the spectrograph slit, typically for minutes in order to catch its spectrum. An example of the Molniya 1-91 and 3-41 reflectance spectra is shown in Fig. 7.

By comparing with the Sun (red dotted spectrum overplotted in the figure) one can appreciate the exceedingly "reddish" color of both Molniyas spacecraft, a feature actually induced by a depleted blue reflectance, shortward of $\lambda \sim 4500$ Å. This is even clearer when analyzing multicolor photometry, especially if we can dig into color details along the satellite rotation. Again, the case of Molniya 1-63 provides a fairly illustrative example in this regard, by

relying on the Loiano multicolor photometry to obtain the (B-R_c) and (R_c-I_c) colors along the lightcurve of Fig. 5 (right panel). Our results are displayed in Fig. 8.

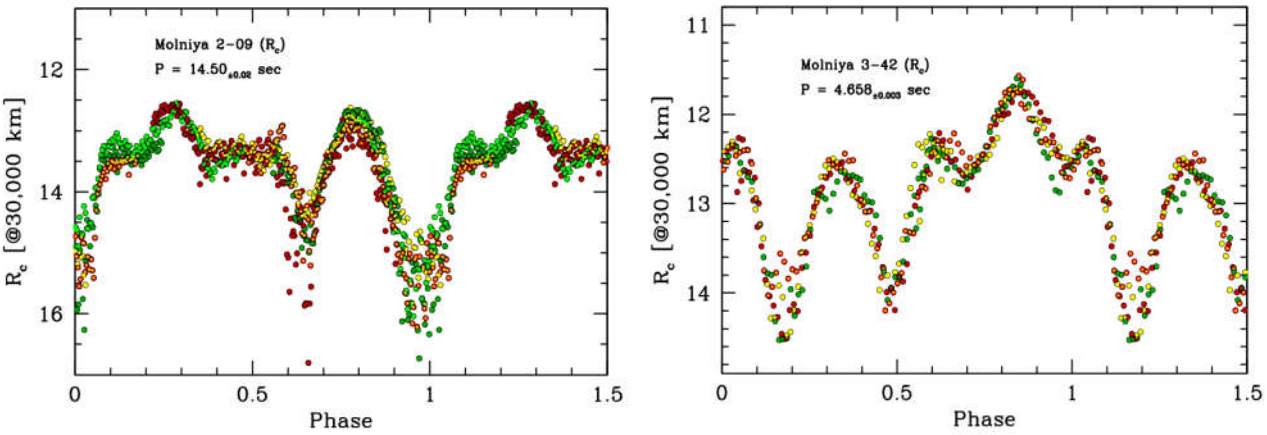

Fig. 6. The R-band lightcurve of Molniya 2-09 (left) and 3-42 (right), respectively as from Cananea observations of 2015 September 20 and Loiano 2014 October 17. The same pattern can easily be recognized in both plots, as a sort of *bona fide* "photometric signature" of Molniya satellites.

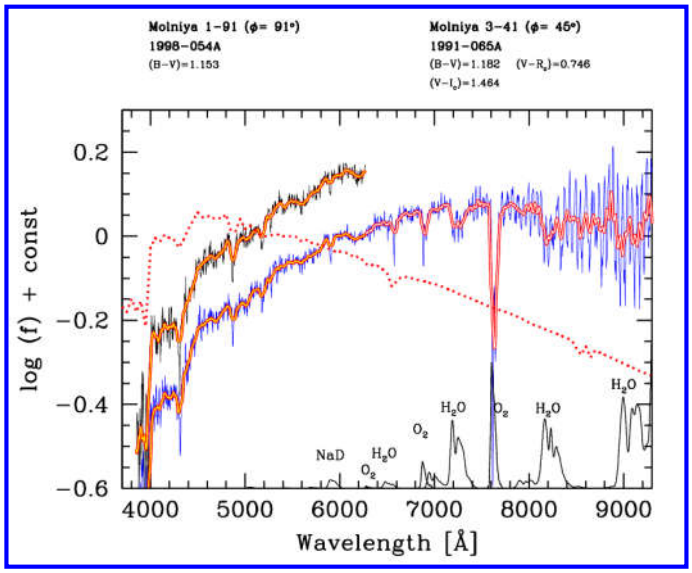

Fig. 7. The reflectance spectra of Molniya 1-91 (black curve) and 3-41 (blue curve), as from BFOSC spectroscopic observations in Loiano. Molniya 1-91 has been observed through grism GR3, while Molniya 3-41 data are from the GR3+GR5 combination (R ~ 400). Both spectra have been smoothed (yellow-red moving average on the plots) for better display. The solar spectrum is overplotted (within arbitrary offset), for comparison (red dotted curve). The absorption features in the satellite spectra are due to the Sun or the telluric absorptions, in the near infrared, mainly by water vapor and Oxygen, as singled out in the lower sketch. Note the fairly "reddish" color of both Molniyas, compared to the Sun.

Along its rotation, the spacecraft wanders in the color plot along a quite entangled path, where we singled out the moments of the two primary (green line) and secondary (red line) maxima (solar pads reflecting), compared with the bus prevailing reflectance (black line). The time-averaged colors are marked by the big blue triangle, while the luminosity-averaged colors are the big yellow triangle. Operationally, the time-averaged colors are likely obtained when probing the spacecraft color with short exposures at random times. On the contrary, luminosity-averaged colors are those we would like to obtain when taking satellite magnitudes over longer exposures, typically exceeding

the spin period. The (R_c-I_c) vs. (B-R_c) locus for Main-Sequence stars of different spectral type, from [15], is also displayed on the plot, for the sake of comparison, by marking Sun's location, as labeled.

It is clearly evident in the plot the exceedingly red color of the bus, and a more marked excursion to the "blue" when solar pads begin to reflect, about the maxima of the lightcurve. Allover, however, we have that the Molniya (R_c-I_c) color closely resembles that of red-dwarf stars of spectral type later than K5. In any case, even considering the (B-R_c) color, the Molniya spacecraft always appear to be redder than the Sun.

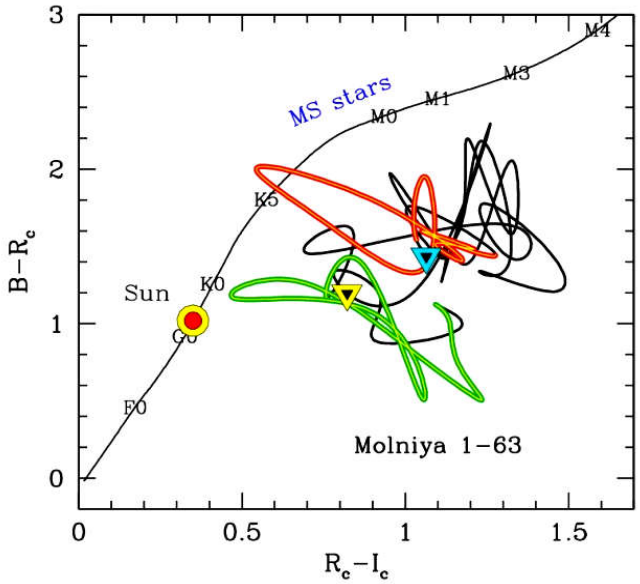

Fig. 8. The observed color path of Molniya 1-63 along its rotation, as from the 2016 Loiano observations (see Fig. 5, right panel) in the (R_c-I_c) vs. (B-R_c) diagram. The lightcurve maxima (that is when solar pads are reflecting) are singled out in green (primary peak) and red (secondary peak), while the black line mainly traces satellite bus reflectance. The big blue and yellow triangles mark respectively the time- and luminosity-averaged colors. For comparison, the (R_c-I_c) vs. (B-R_c) locus for Main-Sequence stars of different spectral type after [15] is also displayed on the plot, marking the Sun's location.

3.4 Dynamical evolution

All the data obtained from the observational campaign will be analyzed in the future to foster an improved synergy between dynamical modeling and real measurements. Here, we will give a first insight on the description that is possible to provide. The available TLE series from the JSPOC/NORAD database [11] cover a significant timespan and it is possible to recognize the main features of the long-term effects due to lunisolar gravitational perturbations, that are, as widely recognized, the dominant perturbations acting on HEO orbits. The second dominant effect on Molniyas' orbital dynamics is certainly the drag, but only when the perigee altitude attains a low enough value. Preliminary analysis shows that this value can be set to 200 km. Recall that due to the high eccentricity and the frozen orbit configuration, the time fraction spent at the perigee is always relatively small.

Focusing on the perigee altitude, it is possible to highlight different periodic components, in particular one of about 7 years and another of about 22 years, the exact value depending on the specific initial conditions of the satellite orbit. In the long term, the third-body effect varies the eccentricity, inclination, longitude of the ascending node Ω and argument of perigee ω, but not the semi-major axis. Thus, as long as the atmospheric drag does not come into play, the minima and maxima that can be noticed in the behavior of the perigee altitude correspond to the maxima and minima in eccentricity, respectively.

To describe such variations, the Lagrange planetary equations applied to the disturbing potential as, for instance, detailed in [16] can be used. Considering the order 2 of the series expansion, that gives the perturbing potential, the equations of motion on the mean orbital elements can be found in [17]. At the inclination of the Molniya orbits, the term yielding the largest growth in eccentricity in the long term is a periodic component whose argument is 2ω. As a

matter of fact, the argument of perigee varies mainly due to the Earth's oblateness and becomes resonant at the critical inclination. By definition, a Molniya orbit fulfills this resonant condition in such a way that, by freezing ω, the spacecraft can spend most of the time at the apogee, hovering the ground stations located in the Northern hemisphere. The periodic components of 7 and 22 years can be imputable, respectively, to the argument (kω+ Ω), where k is an integer ranging in the -3 to 3 interval, depending on the specific value of semi-major axis, and to the harmonic 3ω. As highlighted for instance in [18], for HEO orbits to limit the modeling to the order 2 of the expansion is not sufficient to depict accurately the dynamics.

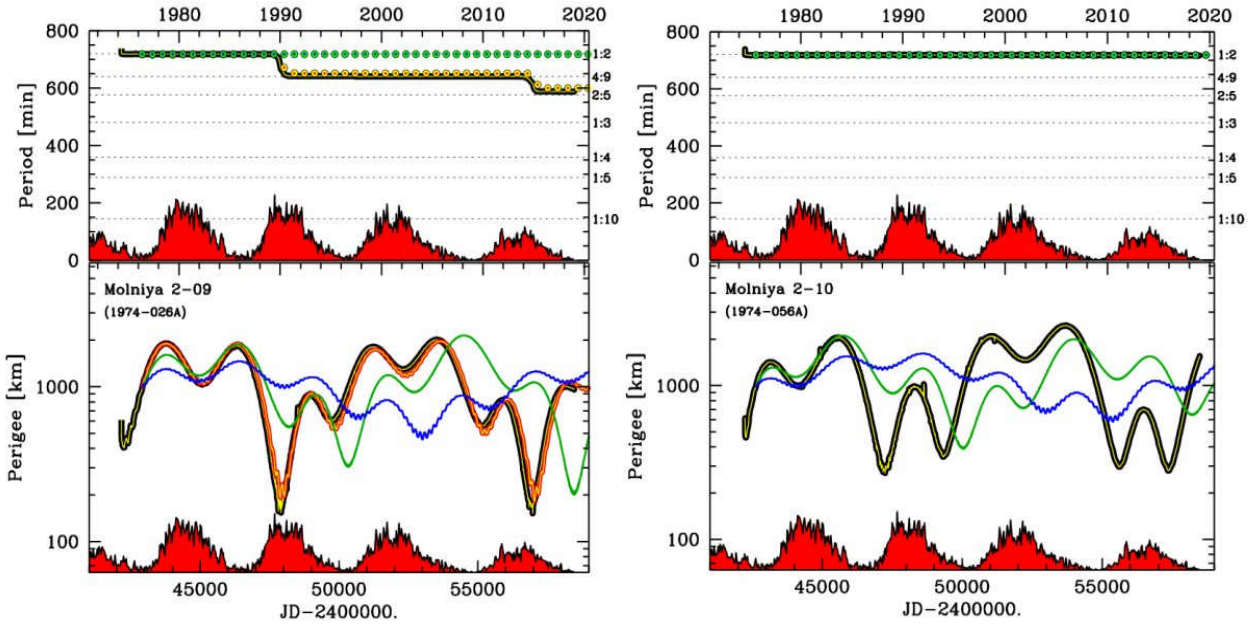

Fig. 9. The historical track of Molniya 2-09 and 2-10, the two oldest satellites in orbit since 1974, are reported according to [11]. Orbit evolution is assessed in terms of drag and lunisolar perturbation acting on the satellite semi-major axis (taking period as a proxy) and eccentricity (with perigee altitude as a proxy). The FOP semi-analytical orbital propagator [19] has been used for our analysis. The historical data are in black, while the Moon and Sun perturbation is singled out, respectively by the green and blue curves and dots. Solar activity is sketched below in each panel (red histogram). Note the 7 and 22-yr "breathing pulse" on satellite eccentricity induced by the lunisolar perturbation, as discussed in the text. For Molniya 2-09 notice as well the period switch, leaving the original 1:2 resonance during two deep excursions of perigee into the atmospheric drag, about year 1990 and 2015. This complex behavior is successfully accounted for by our FOP dynamical model (red-yellow curve and dots on the left panel).

Our dynamical arguments can be discussed here by relying on the historical track of Molniya 2-09 and 2-10, the two oldest satellites survived in orbit, as summarized in Fig. 9. The orbital propagation to obtain the dynamical mapping was carried out by means of the semi-analytical orbital propagator FOP (Fast Orbit Propagator, see [19] for details). Both satellites depart from two very close initial conditions, as reported in Table 1. However, looking at the behavior in eccentricity, or equivalently in perigee altitude, it can be noticed a different evolution.

There are two actors contributing to this. On the one hand, to start at different epochs, displaced by about 3 months, means to have a different contribution from the third-body effect, in particular from the Moon. The first consequence of this is that the first minimum in eccentricity (maximum in perigee altitude) takes place at different epochs and value in the two cases. From that epoch on (MJD 43164 for Molniya 2-10), the maxima and the minima of the two cases are out-of-phase. In particular, the first maximum in eccentricity (minimum in perigee altitude) for Molniya 2-10 occurs about MJD 44221, just after the first minimum in eccentricity for Molniya 2-09. A further consequence is that the deepest perigee altitude in the domain of the atmospheric drag occurs at two different epochs (and thus solar activity, also sketched in the figure) and altitude (namely 280 km for Molniya 2-10 and about 170 km for Molniya 2-09). A second excursion into the drag will take place later with the same features. Very likely, Molniya 2-09 will re-enter sooner than Molniya 2-10.

Table 1 Molniya 2-09 and 2-10 initial conditions (mean orbital elements) as from the TLE historical series

NAME	MJD	a (km)	e	i (deg)	Ω (deg)	ω (deg)
Molniya 2-09	42165.68	27053.96	0.74	62.91	19.58	288.47
Molniya 2-10	42253.13	26982.01	0.74	62.91	270.78	288.47

It should be noticed also that, due to the largest drag effect, the semi-major axis of Molniya 2-09 changes considerably, in particular as much as to move to a different mean motion resonance. While Molniya 2-10 stays in a 1:2 resonance with the Earth's rotation, Molniya 2-09 moves to 4:9 and then to 2:5. In the next future, this kind of considerations will be applied also to the other cases, and will be supported by a theoretical and numerical analysis, paying attention to both the role of Sun and Moon and to the possible occurrence of a chaotic behavior in the timespan considered.

4 REFERENCES

[1] Christopher P., Molniya system alternatives for geostationary satellite systems with applications to 72-100 GHz systems, in Proc. Ka Broadband Conf., Cagliari, Italy, Sep. 2009, p. 1-9, 2009.
[2] Fortescue P., Stark J., Spacecraft system engineering, 2nd Ed. (New York: John Wiley and Sons), p. 132, 1995.
[3] Wiesel W. E., Spaceflight Dynamics, (New York: McGraw-Hill Inc.) p. 86, 1989.
[4] Whitman J. G., Davison W. W., The new hotline - Via satellite direct communications link, Signal, March 1974.
[5] Wade M., 2019, the Astronautix web site at the URL: http://www.astronautix.com
[6] Turkiewicz J. M., NASA compendium of satellite communications programs, CSCL 17B, 1975.
[7] Verger F., Sourbès-Verger I., Ghirardi R., The Cambridge encyclopedia of space, (Cambridge UK: the Cambridge University Press) p. 350, 2003.
[8] N2YO web site at the URL: https://www.n2yo.com
[9] Raushenbakh B. V., Tokar Je N., Attitude control system of Molniya 1 communication satellite, Automatica, Vol. 7, pp. 7-13, 1971.
[10] Buzzoni A., Altavilla, G., Galleti, S., Optical tracking of deep-space spacecraft in Halo L2 orbits and beyond: The Gaia mission as a pilot case, Advances in Space Research, Vol. 57, 1515-1527, 2016.
[11] JSPOC-Celestrak web site at the URL: https://www.space-track.org
[12] Pattan B., Satellite systems: principles and technologies, (New York: Van Nostrand Reinhold), p. 153, 1993
[13] Williams V., Meadows A.. J., Eddy current torques, air torques, and the spin decay of cylindrical rocket bodies in orbit, Planetary and Space Science Vol. 26, 721-726, 1978.
[14] Stellingwerf R. F., Period determination using phase dispersion minimization, The Astrophysical Journal, Vol. 224, 953-960, 1978.
[15] Pecaut M. J., Mamajek E. E., Intrinsic Colors, Temperatures, and Bolometric Corrections of Pre-main-sequence Stars, The Astrophysical Journal Supplement Series 208, 9-22, 2013.
[16] Celletti A., Galeş C., Pucacco G., Rosengren A. J., Analytical development of the lunisolar disturbing function and the critical inclination secular resonance, Celestial Mechanics and Dynamical Astronomy, Vol. 127, pp. 259-283, 2017.
[17] Chao C., Applied Orbit Perturbation and Maintenance, American Institute of Aeronautics and Astronautics/Aerospace Press, Reston, Virginia/El Segundo, California, 2005.
[18] Colombo C., Long-term evolution of highly-elliptical orbits: luni-solar perturbation effects for stability and re-entry, Frontiers in Astronomy and Space Sciences, Vol. 6, 34, 2019.
[19] Rossi A., Anselmo L., Pardini C., Jehn R., Valsecchi G.B., The new space debris mitigation (SDM 4.0) long term evolution code, in: Proceedings of the 5th European Conferences of Space Debris, Darmstadt, Germany, Paper ESA SP-672, 2009.